Check for updates

View Article Online
View Journal

ChemComm
Chemical Communications

Accepted Manuscript

This article can be cited before page numbers have been issued, to do this please use: Y. Xu, H. Wang, J. Zhang, Z. Zhang, M. Liu, X. Tao, J. Zhang and G. Ma, *Chem. Commun.*, 2025, DOI: 10.1039/D5CC03833B.

This is an Accepted Manuscript, which has been through the Royal Society of Chemistry peer review process and has been accepted for publication.

Accepted Manuscripts are published online shortly after acceptance, before technical editing, formatting and proof reading. Using this free service, authors can make their results available to the community, in citable form, before we publish the edited article. We will replace this Accepted Manuscript with the edited and formatted Advance Article as soon as it is available.

You can find more information about Accepted Manuscripts in the Information for Authors.

Please note that technical editing may introduce minor changes to the text and/or graphics, which may alter content. The journal's standard Terms & Conditions and the Ethical guidelines still apply. In no event shall the Royal Society of Chemistry be held responsible for any errors or omissions in this Accepted Manuscript or any consequences arising from the use of any information it contains.

ROYAL SOCIETY OF CHEMISTRY

rsc.li/chemcomm

Please do not adjust margins

ChemComm

View Article Online
DOI: 10.1039/D5CC03833B

COMMUNICATION

A Ta_3N_5/BN composite for enhanced photocatalytic water splitting

Yao Xu, [a] Haifeng Wang, [a] Jiaming Zhang, [a] Zihao Zhang, [a] Meng Liu, [a] Xiaowei Tao, [a] Jifang Zhang, *[a] and Guijun Ma *[a]

Received 00th January 20xx,
Accepted 00th January 20xx

DOI: 10.1039/x0xx00000x

Open Access Article. Published on 03 2025. Downloaded on 04.10.25 15:31:13.
This article is licensed under a Creative Commons Attribution-NonCommercial 3.0 Unported Licence.

Narrow-bandgap Ta_3N_5 nanorods were intensely supported on BN substrate to produce a composite photocatalyst using a NH_4Cl-based vacuum nitridation. The charge separation efficiency of Ta_3N_5 was effectively enhanced due to electron transfer from Ta_3N_5 to the BN substrate, boosting both photocatalytic water oxidation and Z-scheme overall water splitting reactions.

Solar energy conversion into clean hydrogen resource through photocatalytic process is a promising strategy for sustainable energy systems.[1, 2] However, the development of efficient photocatalyst is constrained by limitations in light harvesting, especially in the visible region that takes up 45% of solar spectrum[3], and photon conversion efficiency, restrained by serious bulk and surface charge recombiantions.[4-8] Ta_3N_5 has emerged as a particularly promising photocatalyst due to its bandgap of only 2.1 eV. The conduct band minimum (CBM) and valence band maximum (VBM) of Ta_3N_5 are composed by Ta 5d and N 2p orbitals respectively, thermodynamically allowing for both photocatalytic and photoelectrochemical water redox reactions.[9, 10] In 2002, Hitoki *et al.* reported photocatalytic water oxidation on Ta_3N_5 in presence of an electron acceptor.[11] However, subsequent studies have demonstrated that the performance of Ta_3N_5 is fundamentally limited by issues directly stemming from synthesis method. Specifically, Ta_3N_5 is typically prepared through a NH_3-based thermal nitridation process, which meets challenges including the formation of low-valence metal ions and O_N antisite defects within the crystal structure. These intrinsic defects act as recombination centers that severely suppress charge separation efficiency.[12, 13] Furthermore, high temperature duration leads to particle agglomeration of the products, exacerbating charge recombination issues. As a consequence of these synthesis-related challenges, Ta_3N_5 exhibits unsatisfactory photon conversion efficiencies in photocatalytic reactions.[14-16]

Nanostructural engineering, by precisely controlling the morphology and architecture of oxide precursors, has emerged as an effective strategy to improve charge separation efficiency in Ta_3N_5 photocatalysts by reducing charge transport distances and extending carrier lifetimes.[17] Ma *et al.* applied Ta_2O_5 and Na_2CO_3 mixture to produce $NaTaO_3/Ta_2O_5$ composite, which was then used as precursor for thermal ammonlysis. This method suppressed Ta_3N_5 agglomeration and enhanced crystallinity.[14] Wang *et al.* prepared Ta_2O_5 coated Pt/SiO_2 nanoparticles for the fabrication of hollow Ta_3N_5 nanoshell, subsequently loading CoO_x onto the outer surface of Ta_3N_5 and Pt left on inner shell after removing SiO_2.[18] The nanoshell structure not only provided a structural framework for efficient charge transport but also facilitated directional carrier extraction by spatially separating reduction and oxidation cocatalysts, thus boosting charge separation. Wang *et al.* applied $KTaO_3$ as vaporous Ta resource to produce Ta_3N_5 nanorod single crystals and accelerate heat ammonium flow reduced the duration of nitridation process. The highly crystallized Ta_3N_5 nanorods with fewer defects realized one-step excitation overall water splitting reaction under visible light illumination.[9] Nanostructured precursors enable controlled Ta_3N_5 particle morphology, effectively decreasing agglomeration and shortening carrier transport distances, while structuring catalyst/host interface promotes more efficient carrier transport, enhancing charge separation efficiency and thereby unlocking Ta_3N_5's potential for photocatalysis.

Our group has developed a NH_4Cl-based vacuum nitridation method to synthesize transition metal (oxy)nitrides such as Ta_3N_5/Ta thin film,[19] TaON powders[20] and ZnO:GaN nanoparticles.[21, 22] For the preparation of the Ta_3N_5/Ta thin film,

[a] School of Physical Science and Technology, ShanghaiTech University, Shanghai 201210, China.

† Supplementary Information available: [details of any supplementary information available should be included here]. See DOI: 10.1039/x0xx00000x

ChemComm Accepted Manuscript

Open Access Article. Published on 03 2025. Downloaded on 04.10.25 15:31:13.
This article is licensed under a Creative Commons Attribution-NonCommercial 3.0 Unported Licence.

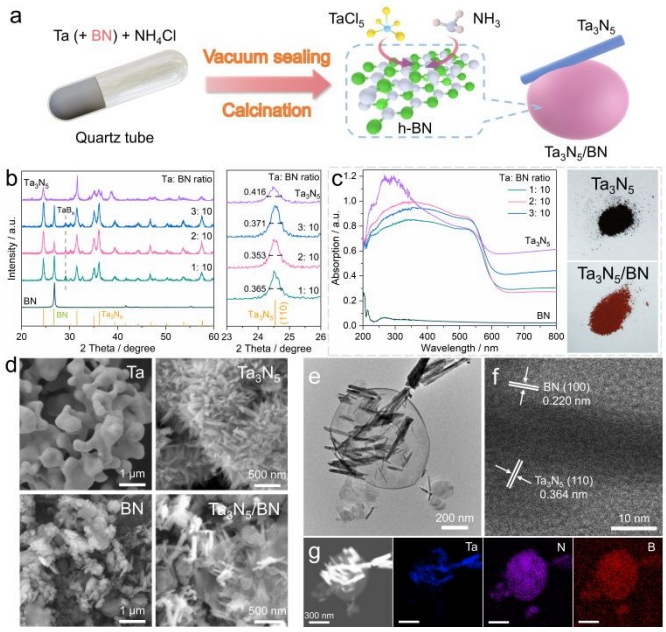

Figure 1. (a) Illustration of the synthesis of Ta_3N_5/BN composite. (b) XRD patterns of BN precursor, bulk Ta_3N_5, and the Ta_3N_5/BN samples prepared from different Ta/BN ratios. (c) UV-vis DRS of BN, Ta_3N_5, and Ta_3N_5/BN powders as well as digital images of Ta_3N_5 and Ta_3N_5/BN (Ta:BN = 2:10) samples. (d) SEM images of Ta and BN precursors and corresponding Ta_3N_5 and Ta_3N_5/BN products. (e) TEM, (f) HRTEM, (g) dark field image and EDS mapping images of Ta_3N_5/BN (Ta:BN = 2:10) sample. The referenced patterns of BN and Ta_3N_5 in (b) are ICDD-00-045-1171 and ICDD-04-004-4564, respectively.

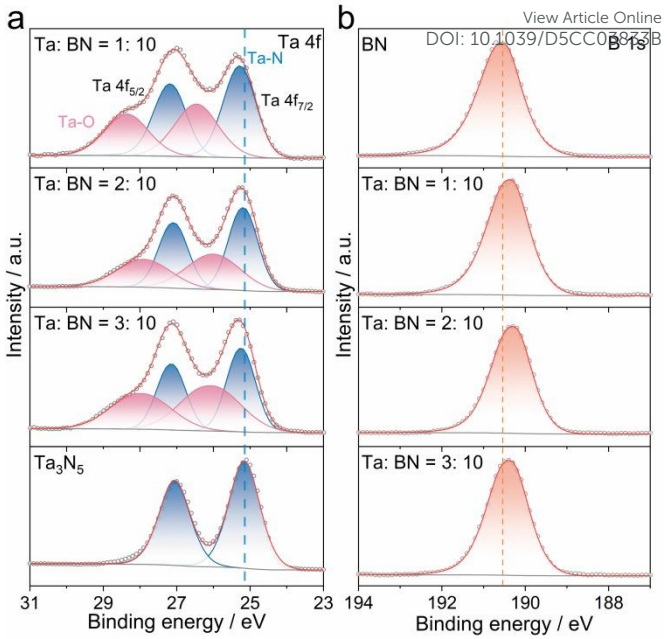

View Article Online
DOI: 10.1039/D5CC03873B

Figure 2. XPS of the Ta_3N_5/BN samples prepared from different precursor ratios with including Ta_3N_5, BN for reference. (a) Ta 4f, and (b) B 1s spectra.

only Ta wafer and NH_4Cl are used as precursors. Upon heating, in the first step, NH_3 and HCl are produced from the decomposition of NH_4Cl. The metallic Ta reacts with HCl to produce a gaseous $TaCl_5$ intermediate, which subsequently reacts with NH_3 to form Ta_3N_5 particles on the surface of Ta plate. The high permeability of gaseous $TaCl_5$ and NH_3 reactants not only leads to a fast crystallization of the solid product, but also prevents Ta_3N_5 from forming reduced Ta species by limited exposure to NH_3 atmosphere.

Herein, we introduced a two-dimensional BN as substrate for growth of Ta_3N_5 nanoparticles in the NH_4Cl-based nitridation process. The involvement of BN in precursor led to improved crystallinity and dispersion of the Ta_3N_5 particles. Reductive photodeposition of Ag and Rh suggested that electrons were transferred from Ta_3N_5 to BN under irradiation. Such directional charge migration greatly enhanced photocatalytic activities of Ta_3N_5 for water splitting, highlighting the benefits of photocatalyst-substrate interaction.

The Ta_3N_5 bulk and Ta_3N_5/BN composite were synthesized by vacuum sealing a mixture of NH_4Cl and metallic Ta powders in a quartz tube with or without adding BN (Fig. 1a with details shown in Supporting Information). For Ta_3N_5/BN, the atomic ratios of Ta:BN were set as 1:10, 2:10 and 3:10, respectively. Fig. 1b displays the X-ray diffraction (XRD) patterns of the powders prepared from different Ta:BN ratios. All the BN-containing samples exhibit patterns of mixed BN and Ta_3N_5 peaks, with a weak signal at ~29° assigning to TaB_x impurities. The majority peaks of Ta_3N_5/BN are consistent with standard Ta_3N_5 patterns, indicating the high purity of Ta_3N_5 in obtained samples. No signals of metallic Ta are observed in the products. Additionally, the full width half maximum (FWHM) of Ta_3N_5 (110) diffraction peaks in Ta_3N_5/BN samples are lower than that of Ta_3N_5, indicating enhanced crystallinity of Ta_3N_5 when BN is presented during synthesis. Fig. 1c shows the UV-vis diffuse reflectance spectroscopy (DRS) of BN, Ta_3N_5 and Ta_3N_5/BN powders. The BN precursor exhibits negligible UV-visible light absorption due to its wide bandgap of 5.1 eV. Ta_3N_5 reference powder shows a broad absorption up to 600 nm corresponding to its bandgap (2.1 eV). The observed dark brown color, as opposed to dark red, can be attributed to elevated absorption in the near-infrared region. All Ta_3N_5/BN samples exhibit smooth band-to-band absorption features typical of Ta_3N_5, revealing that optical property of Ta_3N_5 is not changed with the introduction of BN in precursor as corroborated by the Tauc plots in Fig. S1. Compared to Ta_3N_5, the relatively lower background levels above 600 nm for the Ta_3N_5/BN samples suggest less absorption associated with intragap defect states. Notably, the Ta:BN = 2:10 sample achieves the strongest light absorption, showing that photon absorption is not linearly increased with higher Ta ratio in precursor.

Scanning electron microscopy (SEM) images (Fig. 1d) display morphology of the precursors and nitridation products. Without incorporating BN during nitridation, large Ta precursor particles are converted into aggregated Ta_3N_5 nanorods. In the presence of BN, the nitridation products show more uniformly distributed and well-isolated Ta_3N_5 particles dispersed on the BN substrate. SEM images of different Ta_3N_5/BN samples (Fig. S2) in back scattered electron (BSE) mode show that the dispersity of Ta_3N_5 nanorods in the Ta: BN = 2: 10 sample are higher than that in the 1: 10 and 3:10 samples. It demonstrates that Ta content can effectively impacts on the growth of Ta_3N_5 particles, highlighting

ChemComm Accepted Manuscript

 This journal is © The Royal Society of Chemistry 20xx

View Article Online
DOI: 10.1039/D5CC03833B

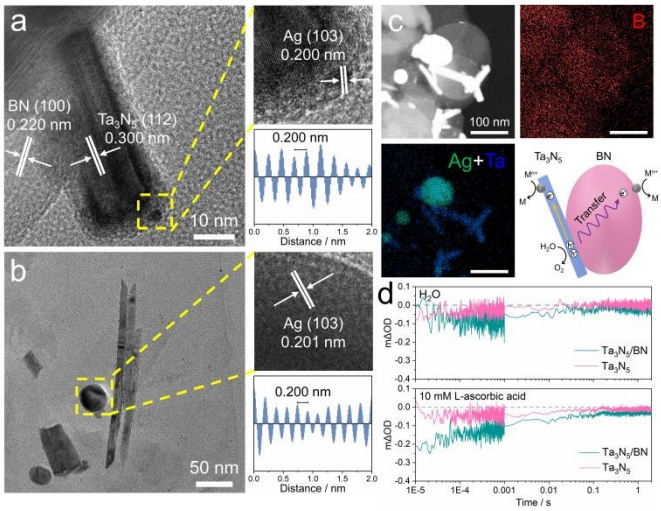

Figure 3. HRTEM images and lattice fringe distances of Ag particles loaded on (a) Ta_3N_5 and (b) BN in Ta_3N_5/BN particles. (c) Dark field image, EDS mappings and structure diagram of Ta_3N_5/BN sample loaded with Ag. (d) Transient absorption spectrum for Ta_3N_5 and Ta_3N_5/BN in water without (top panel) or with L-ascorbic acid (bottom panel). The pump and probe lights in (d) are 355 and 580 nm, respectively. The Ta_3N_5/BN sample is prepared from a Ta:BN = 2:10 ratio.

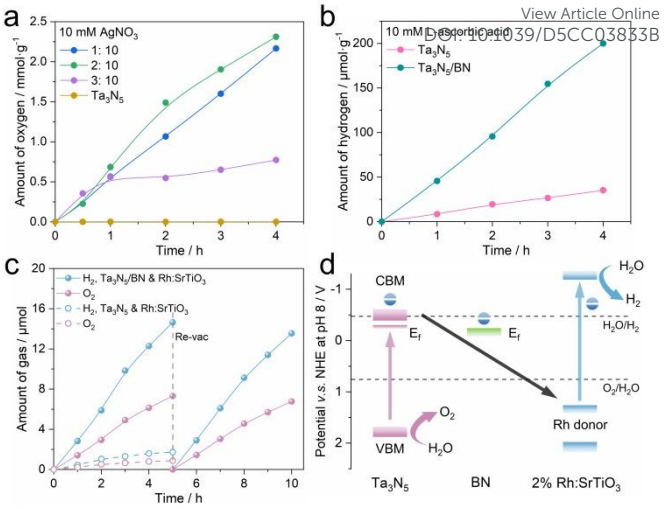

Figure 4. (a) Time profiles of photocatalytic OER on Ta_3N_5/BN and bulk Ta_3N_5 samples in $AgNO_3$ reagent. (b) HER activities of Ta_3N_5/BN and Ta_3N_5 in L-ascorbic acid reagent. (c) H_2 and O_2 production from physical oscillation between Ta_3N_5/BN and 2% Rh:$SrTiO_3$ at pH 5. (d) Diagram of Z-scheme electron transfer between Ta_3N_5/BN and Rh:$SrTiO_3$. The Ta_3N_5/BN in (b) and (c) are prepared from a Ta:BN = 2:10 ratio and each assessment applied 30 mg catalyst. 0.75 wt% IrO2 and 1 wt% Pt was loaded as cocatalyst for OER and HER, respectively.

the NH_4Cl-based vacuum nitridation a potential method for constructing regulated nanostructures. Transmission electron microscopy (TEM) image of Ta:BN = 2:10 sample (Fig. 1e) shows that Ta_3N_5 nanorods with lengths around hundreds of nanometers lying on BN substrate. The BN structure remains unchanged after the high-temperature nitridation. The TEM image clearly demonstrates that Ta_3N_5 particles in obtained samples adopt a typical nanorod morphology, which is similar to those Ta_3N_5 particles prepared directly from $TaCl_5$ and NH_3 precursors.[23] High resolution TEM (HRTEM) image in Fig. 1f exhibits the interface of Ta_3N_5 and BN particles. The close stacking of 0.364 nm lattice fringes assigning to (110) facet of Ta_3N_5 and 0.220 nm lattice fringes assigning to BN (100) facet suggests the growth of Ta_3N_5 on BN substrate. Fig. 1g shows the TEM dark field image and energy dispersive X-ray spectroscopy (EDS) of Ta: BN = 2: 10 sample. The overlapped N and Ta signals further confirm the nanorod morphology of Ta_3N_5 on BN substrate.

XPS analysis was carried out on Ta_3N_5, BN and Ta_3N_5/BN particles. The well-defined double peaks at 25.2 and 27.1 eV (Fig. 2a) assigning to Ta $4f_{7/2}$ and $4f_{5/2}$ in Ta_3N_5 reveal that the NH_4Cl-based nitridation suppresses the formation of reduced Ta species. For Ta_3N_5/BN particles, additional double peaks are observed at high field shift, which is supposed to be TaO_x impurities.[24] O 1s spectrum (Fig. S3) reveals the existence of crystalline O species in Ta_3N_5 and Ta_3N_5/BN, suggesting surface coverage of those TaO_x species. Besides, compared with Ta_3N_5, a slightly higher binding energy of Ta^{5+} signals in Ta-N of Ta_3N_5/BN samples reflects a possible electron transfer from Ta_3N_5 to BN. Relative to BN, the lower shift in B 1s binding energy for Ta_3N_5/BN samples also suggests an interfacial electron transfer between two components (Fig. 2b).

To verify electron transfer between Ta_3N_5 and BN under illumination, visible light-driven photoreduction of Ag^+ ions was

Ag particles are loaded on the Ta_3N_5/BN composite photocatalyst. The 0.200 nm lattice fringes attributing to Ag (103) facet are observed on both BN and Ta_3N_5 particles. The EDS mappings in Fig. 3c clearly distinguishes the Ag nanoparticles loaded away from Ta_3N_5 nanorods. Considering that BN barely absorbs visible light, it indicates that photogenerated electrons are partially transferred from Ta_3N_5 to BN, as illustrated in structure diagram of Fig. 3c. As a further evidence, by using Rh^{3+} as a precursor, Rh nanoparticles can also be reductively photodeposited on the BN substrate (Fig. S4). Mott-Schottky analysis and valance spectra (Fig. S5) reveal that the Fermi level of BN is closely aligned with that of Ta_3N_5. Such energetic alignment is beneficial for electron transfer from Ta_3N_5 to BN.

Transient absorption spectroscopy was employed to investigate the electron transfer from Ta_3N_5 to BN under light excitation and in solution. The pump and probe lights were set at 355 and 580 nm, respectively. For BN alone (Fig. S6), no meaningful transient absorption signal is observed as its band gap exceeds the pump light wavelength. On the other hand, both Ta_3N_5 and Ta_3N_5/BN show a weak negative absorption at 580 nm (Fig. 3d). To assign this signal, L-ascorbic acid is added as a hole scavenger. Here, the intensity of the negative absorption increases for both samples, confirming that such signal is associated with photogenerated electrons. It is worth noting that the negative absorption for Ta_3N_5/BN is significantly stronger than that for Ta_3N_5, indicating superior charge carrier separation in the former sample.

The catalyst-substrate electron transfer in Ta_3N_5/BN is supposed to promote its photocatalytic performance *via* improving electron-hole separation. Fig. 4a displays the activities of photocatalytic oxygen evolution reaction (OER) on Ta_3N_5 or Ta_3N_5/BN in presence of $AgNO_3$ as an electron scavenger. An IrO_2 species is loaded on the catalysts to assist

Open Access Article. Published on 03 2025. Downloaded on 04.10.25 15:31:13.
This article is licensed under a Creative Commons Attribution-NonCommercial 3.0 Unported Licence.
ChemComm Accepted Manuscript

Open Access Article. Published on 03 2025. Downloaded on 04.10.25 15:31:13. This article is licensed under a Creative Commons Attribution-NonCommercial 3.0 Unported Licence.

the OER process (Fig. S7). The Ta_3N_5 nanorods barely produce oxygen due to rapid passivation by Ag coverage on its active sites.[23] However, Ta_3N_5/BN exhibit linear oxygen evolution in the early stages, revealing that electron interaction slows down the Ag passivation and preserves photocatalytic activity. Among Ta_3N_5/BN products, the Ta:BN = 2:10 sample has the highest water oxidation rate. It is likely due to better photon absorption (Fig. 1c) and the more uniform distribution of Ta_3N_5 nanorods on BN substrate (Fig. S2) for this sample.

Fig. 4b displays photocatalytic hydrogen evolution (HER) on Ta_3N_5/BN (Ta:BN = 2:10) and Ta_3N_5 assisted with L-ascorbic acid as a hole sacrificial reagent. Pt (1 wt%) is optimized as the HER cocatalyst (Fig. S7). The Ta_3N_5/BN composite structure also shows a considerably enhanced hydrogen evolution rate compared with Ta_3N_5 nanorods, despite a much lower HER rate compared to OER. This highlights the thermodynamic limitations of Ta_3N_5/BN for proton reduction (Fig. S8). To break such limitation, Fig. 4c displays a Z-scheme overall water splitting reaction by physical collision between Ta_3N_5/BN and Rh doped $SrTiO_3$ (Rh:$SrTiO_3$) particles. Under visible light illumination, stoichiometric hydrogen and oxygen evolution over 10 h is realized for Ta_3N_5/BN, while the Ta_3N_5 exhibits significantly lower activity. Fig. 4d represents the band structure of Ta_3N_5/BN and Rh:$SrTiO_3$ determined from Mott-Schottky and bandgap assessment in Fig. S9. It is obvious that transfer of photogenerated electrons from Ta_3N_5 to BN favors the Z-scheme electron transfer pathway, effectively overcoming the insufficient reduction driving force of Ta_3N_5/BN.

In summary, a Ta_3N_5/BN composite photocatalyst is synthesized *via* the NH_4Cl-based vacuum nitridation process. The Ta_3N_5 component exhibits highly crystallized nanorod morphology during growth on the BN substrate. Photodeposition of Ag metal, chemical state analysis and carrier dynamics assessment confirm electron transfer between Ta_3N_5 and BN. Enhanced photocatalytic performance in water splitting emphasizes the promotion of charge separation efficiency by electron interaction of catalyst/substrate interface. Our work not only provides a new method for synthesizing highly crystalized Ta_3N_5 nanorods but also demonstrates an efficient composite structure for enhancing the photocatalytic performance of this promising photocatalyst.

This work was financially supported by the National Natural Science Foundation of China (22572123), Shanghai Natural Science Foundation of China (24ZR1451400), Starting Foundation of ShanghaiTech University, and Double First-Class Initiative Fund of ShanghaiTech University. J.F. Zhang acknowledges financial support from the Shanghai Rising-Star Program (Yangfan Special Project, 24YF2729000), the Science and Technology Commission of Shanghai Municipality (STCSM). We also thank the support from Analytical Instrumentation Center (no. SPST-AIC10112914) and CħEM (no. EM02161943), SPST of ShanghaiTech University.

Conflicts of interest

View Article Online
DOI: 10.1039/D5CC03833B

There are no conflicts to declare.

Data availability

The data supporting this article have been included as part of the ESI.

Notes and references

1 W. Wang, X. Xu, W. Zhou and Z. Shao, *Adv. Sci.*, 2017, **4**.
2 Q. Yang, X. Tong and Z. Wang, *Mater. Rep.: Energy*, 2024, **4**.
3 Q. Wang and K. Domen, *Chem. Rev.*, 2020, **120**, 919-985.
4 Q. Wang, C. Pornrungroj, S. Linley and E. Reisner, *Nat. Energy*, 2021, **7**, 13-24.
5 S. Ye, W. Shi, Y. Liu, D. Li, H. Yin, H. Chi, Y. Luo, N. Ta, F. Fan, X. Wang, et al., *J. Am. Chem. Soc.*, 2021, **143**, 12499-12508.
6 M. S. Prévot and K. Sivula, *J. Phys. Chem. C*, 2013, **117**, 17879-17893.
7 J. H. Kim, J. W. Jang, Y. H. Jo, F. F. Abdi, Y. H. Lee, R. van de Krol and J. S. Lee, *Nat. Commun.*, 2016, **7**, 13380.
8 L. Pan, J. H. Kim, M. T. Mayer, M.-K. Son, A. Ummadisingu, J. S. Lee, A. Hagfeldt, J. Luo and M. Grätzel, *Nat. Catal.*, 2018, **1**, 412-420.
9 Z. Wang, Y. Inoue, T. Hisatomi, R. Ishikawa, Q. Wang, T. Takata, S. Chen, N. Shibata, Y. Ikuhara and K. Domen, *Nat. Catal.*, 2018, **1**, 756-763.
10 Y. Q. Xiao, C. Feng, J. Fu, F. Z. Wang, C. L. Li, V. F. Kunzelmann, C. M. Jiang, M. Nakabayashi, N. Shibata, I. D. Sharp, et al., *Nat. Catal.*, 2020, **3**, 932-940.
11 G. Hitoki, A. Ishikawa, T. Takata, J. N. Kondo, M. Hara and K. Domen, *Chem. Lett.*, 2002, **31**, 736-737.
12 G. Fan, T. Fang, X. Wang, Y. Zhu, H. Fu, J. Feng, Z. Li and Z. Zou, *iScience*, 2019, **13**, 432-439.
13 J. Fu, F. Wang, Y. Xiao, Y. Yao, C. Feng, L. Chang, C.-M. Jiang, V. F. Kunzelmann, Z. M. Wang, A. O. Govorov, et al., *ACS Catal.*, 2020, **10**, 10316-10324.
14 S. S. Ma, T. Hisatomi, K. Maeda, Y. Moriya and K. Domen, *J. Am. Chem. Soc.*, 2012, **134**, 19993-19996.
15 K. N. Sun, Y. Y. Li, Q. G. Zhang, L. Wanga, J. L. Zhang and X. Zhou, *Appl. Surf. Sci.*, 2017, **405**, 289-297.
16 X. Wang, H. Huang, G. Fan, Z. Li and Z. Zou, *J. Phys. Chem. C*, 2017, **122**, 489-494.
17 M. Xiao, S. C. Wang, S. Thaweesak, B. Luo and L. Z. Wang, *Engineering*, 2017, **3**, 365-378.
18 D. Wang, T. Hisatomi, T. Takata, C. Pan, M. Katayama, J. Kubota and K. Domen, *Angew. Chem., Int. Ed.*, 2013, **52**, 11252-11256.
19 Y. Xiang, B. Zhang, J. Liu, S. Chen, T. Hisatomi, K. Domen and G. Ma, *Chem. Commun.*, 2020, **56**, 11843-11846.
20 Y. Xu, K. Liu, J. Zhang, B. Zhang, J. Zhang, K. Shi, H. Wang and G. Ma, *J. Energy Chem.*, 2024, **94**, 541-550.
21 K. Liu, B. Zhang, J. Zhang, W. Lin, J. Wang, Y. Xu, Y. Xiang, T. Hisatomi, K. Domen and G. Ma, *ACS Catal.*, 2022, DOI: 10.1021/acscatal.2c04361, 14637-14646.
22 K. Liu, B. Zhang, J. Zhang, Y. Xu, J. Zhang, Z. Zhang, K. Shi, N. Wang, S. Chen and G. Ma, *ACS Catal.*, 2024, **14**, 10138-10147.
23 D. L. Lu, M. Hara, T. Hisatomi, T. Takata and K. Domen, *J. Phys. Chem. C*, 2009, **113**, 17151-17155.
24 M. Li, W. Luo, D. Cao, X. Zhao, Z. Li, T. Yu and Z. Zou, *Angew. Chem. Int. Ed.*, 2013, **52**, 11016-11020.

ChemComm Accepted Manuscript

View Article Online
DOI: 10.1039/D5CC03833B

Data availability

The data supporting this article have been included as part of the ESI.

Open Access Article. Published on 03 2025. Downloaded on 04.10.25 15:31:13.
This article is licensed under a Creative Commons Attribution-NonCommercial 3.0 Unported Licence.

ChemComm Accepted Manuscript